Principle and application of low energy inverse photoemission spectroscopy: A new method for measuring unoccupied states of organic semiconductors

Hiroyuki Yoshida

Graduate School of Advance Integration Science, Chiba University, 1-33 Yayoi-cho, Inage-ku, Chiba 263-8522, Japan

TEL: +81-43-290-2958
FAX: +81-43-207-3896
Email: hyoshida@chiba-u.jp

Abstract

Information about the unoccupied states is crucial to both fundamental and applied physics of organic semiconductors. However, there were no available experimental methods that meet the requirement of such research. In this review, we describe a new experimental method to examine the unoccupied states, called low-energy inverse photoemission spectroscopy (LEIPS). An electron having the kinetic energy lower than the damage threshold of organic molecules is introduced to a sample film, and an emitted photon in the near-ultraviolet range is detected with high resolution and sensitivity. Unlike the previous inverse photoemission spectroscopy, the sample damage is negligible and the overall resolution is a factor of two improved to 0.25 eV. Using LEIPS, electron affinity of organic semiconductor can be determined with the same precision as photoemission spectroscopy for ionization energy. The instruments including an electron source and photon detectors as well as application to organic semiconductors are presented.

Keywords

low-energy inverse photoemission spectroscopy; unoccupied state; electron affinity; organic semiconductor;

1. Introduction

Both holes and electrons play a crucial role in electronic properties of organic semiconductors. Thus it is equally important to investigate the occupied and unoccupied states of organic solids. The occupied states have been extensively studied using photoemission spectroscopy (PES). PES is a surface sensitive technique and can be applied to organic thin films to examine the density of occupied states with reference to the Fermi and vacuum levels. A momentum resolved (*k*-resolution) measurement is also possible by measuring the dependencies of the energy of excitation photons or angle of emitted electron. Taking advantage of these properties of UPS, interface energy level alignments [1, 2], energy band dispersion[3], and molecular orientation dependence of ionization energy [4] have been reported so far.

In contrast, little is known about the unoccupied states because of limitation of experimental technique available. Several methods have been used for the unoccupied states of organic materials, such as X-ray absorption spectroscopy, combination of ultraviolet-visible spectroscopy and PES, scanning tunneling spectroscopy (STS), cyclic voltammetry (CV) and inverse photoemission spectroscopy (IPES)[5,6]. In principle, IPES is complementary to PES for occupied states and is only capable of quantitatively analyzing unoccupied states of solid samples with surface sensitivity and *k*-resolution.

Figure 1 shows the principle of IPES. An electron having a kinetic energy E_k is introduced to a sample surface and a photon with energy $h\nu$ emitting as a result of the radiative transition to an unoccupied state is detected. The electron binding energy E_b is determined based on the energy conservation, $E_b = h\nu - E_k$. The IPES spectrum is measured either by sweeping an electron kinetic energy E_k with detecting photons at a fixed energy $h\nu$, called the isochromat mode, or by analyzing the photon energy $h\nu$ at a constant electron kinetic energy E_k, called the tunable photon energy (TPE) mode.

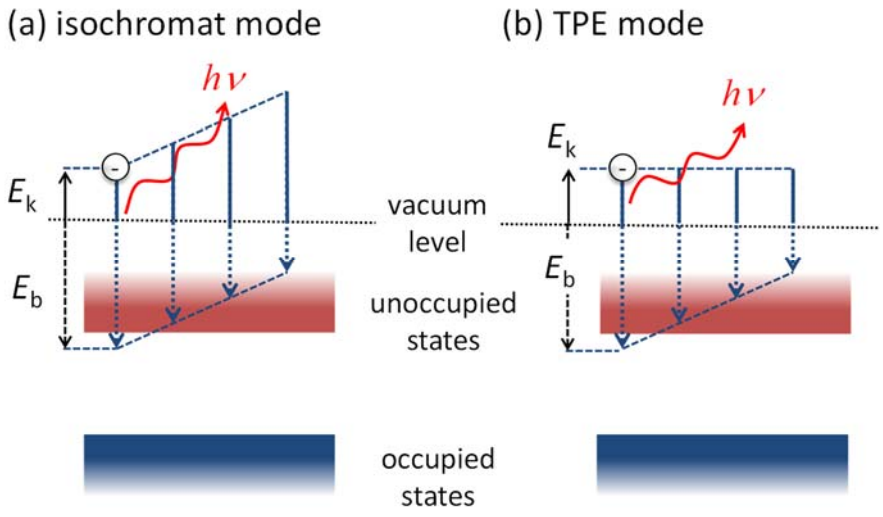

Fig. 1: Principle of inverse photoemission spectroscopy. a) Electron kinetic energy E_k is scanned with detecting photons at a fixed energy $h\nu$ (isochormat mode). b) Electron kinetic energy E_k is fixed and photons with various energies are analyzed using a spectrometer (TPE mode).

IPES was first applied to organic materials in 1980s [7-11]. Molecules adsorbed on single crystalline surfaces of metals were observed and the unoccupied molecular orbitals were identified by comparing with the molecular orbital calculations. Larger number of research groups started IPES around 2000 in connection with the fundamental and applied studies toward organic electronics [12-17]. However, the obtained results from IPES were disappointing. Organic samples were found to be easily degraded by the electron bombardment [18, 19] and the energy resolution was as high as 0.5 eV that is substantially lower than PES [20]. In Figure 2a compares the first and second scans of the IPES spectra of hexatriacontane (n-$C_{36}H_{74}$) at the incident electron density of 1.1 x 10^{-3} A m^{-2}. [18] The peak at 2.5 eV in the first scan shifts to 4 eV in the second scan demonstrating that the sample is seriously damaged by the electron bombardment during the measurement. Figure 2b shows the combined UPS [21] and IPES [22] spectra (the energy resolution is 0.8 eV) of copper phthalocyanine (CuPc) . Apparently, the onset region is not clear in the IPES spectrum owing to the low energy resolution.

The difficulties of IPES originate from the inherently low signal intensity. The cross section of IPES is 3 or 5 orders magnitude smaller than that of PES [23]. In order to gain a sufficient signal-to-noise ratio, an intense electron beam is introduced to a sample resulting in the sample damage. The photon is analyzed with a specially designed detector which is optimized to gain high sensitivity and lose the energy resolution.[24]

Recently, we have developed low-energy inverse photoemission spectroscopy (LEIPS) [25]. This new technique have solved the issues of the previous IPES simultaneously by using electron beam having the kinetic energy lower than the damage threshold of organic materials. In this review, we present the principle, instruments, performance of LEIPS followed by several applications to the organic semiconductors.

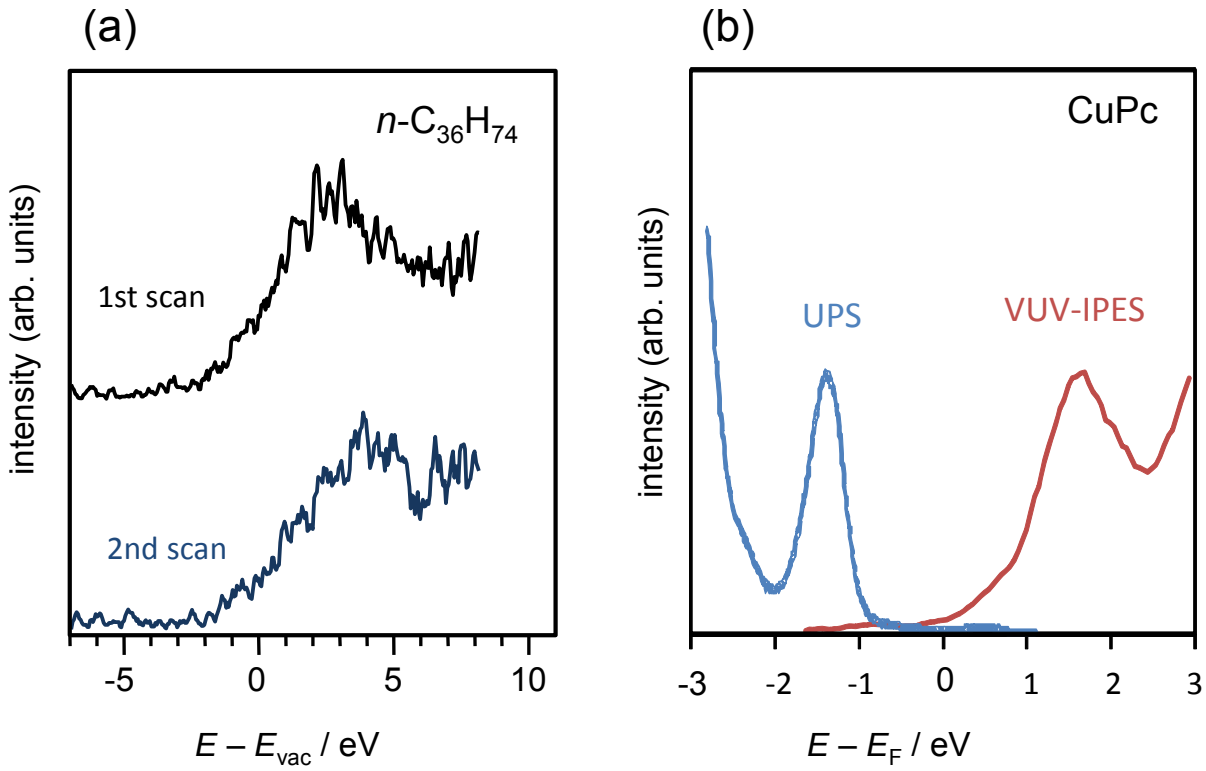

Fig. 2: Spectra of the previous IPES (VUV-IPES) demonstrating that a) organic samples are damaged during the first scan,[18] and b) the energy resolution is substantially lower than that of ultraviolet photoemission spectroscopy (UPS). [22]

2. Basic idea of low-energy inverse photoemission spectroscopy

IPES was first pursued in the X-ray range since 1940s (see Ref[26]). Studies of IPES in the vacuum ultraviolet (VUV) range started with the introduction of the bandpass photon detector using the Geiger-Müller tube and optical filter in 1970s [24, 27]. The iodine gas-filled Geiger- Müller serves as the high pass filter with the sensitivity beyond 9.2 eV and the optical filter of CaF_2 as low pass filter with the cut-off energy of 10 eV making a bandpass sensitivity centered at 9.7 eV with the half-width at maximum (FWHM) of 0.7 eV. This VUV photon detector has high quantum efficiency and large

solid angle of the photon collection as well as is easy to construct. This work established IPES as a standard spectroscopic technique for surface science. Here, we call this experimental method as VUV-IPES. The energy resolution has been improved by changing the filled gases and the optical filters [28-34]. The Geiger-Müller tube was replaced with a solid state detector to improve the stability of operation [35-37]. Most of the IPES studies of organic materials have been conducted using the bandpass detector so as to minimize the sample damage. The disadvantage is low-flexibility of bandpass property because the bandpass sensitivity is obtained by the combination of the photon-sensitive and filter materials. The center of the passband is always around 10 eV, and the energy resolution is as high as 0.5 eV for a practical sensitivity.

For the analysis of photons in the VUV range, spectrometers have been also used [38-46]. However, these spectrometers were low in the photon detection efficiency because of the low reflectivity of gratings in the VUV range and the small solid angel of photon collection. The application to organic materials was thus limited to the highly durable molecules such as fullerenes [47, 48].

Since the electron affinity of organic semiconductors mostly falls in the range between 2 and 5 eV [49, 50], the energy of incident electron ranges between 5 and 15 eV when the VUV photons are detected by the bandpass photon detector. The electron beam in this energy range causes serious damage to organic samples. The damage threshold of organic materials is reported to about 5 eV [51] which corresponds to the energy of covalent bonds of organic molecules. If the energy of electron is lowered below 5 eV, the sample damage is expected to be reduced. In this case, the photon energy is estimated to be less than 5 eV, i.e, the near ultraviolet range (NUV). Basically, the NUV photons can be analyzed easier than the VUV photons leading to the higher resolution and sensitivity. The two issues of previous VUV-IPES can, therefore, be solved simultaneously by lowering the electron energy.

3. Instruments

Based on the idea described above, we have developed instruments consisting of an electron source and a photon detector. In this section, the performance of LEIPS is also demonstrated focusing on the sample damage and energy resolution.

3-1 Electron source

For the low-energy electron source, we used an electron gun originally designed by

Erdman and Zipf [52] after modifications (Figure 3a). In order to decrease the thermal spread of electron energy, the tungsten filament was replaced with the barium oxide (BaO) cathode. This cathode operates at about 1100 K and the thermal spread of electron is estimated to about 0.25 eV.

According to the original literature, this electron gun generates a parallel electron beam while we need to optimize the spot size of electron beam on the sample. The photons from the sample are focused into the photon detector using a lens as mentioned later. The spot size of the electron on the sample determines the object size of the optical system while the image size is determined by diameter of a bandpass filter or width of the entrance slit of a spectrometer. Considering the efficient focusing of the photons into the photon detector, the small spot size is preferable. On the other hand, low electron density is desirable to eliminate charging of and damage to the organic samples.

We found the spot size of electron beam can be adjusted by varying the electrostatic potential of the last electrode (denoted D in Figure 3). The beam diameter was examined at 20 mm downstream from the exit aperture of the electron gun using a phosphor screen. The results are shown in Figure 3b. In the original design, the potential of the electrode D is 4 times of the beam energy V_0. By increasing the potential up to V_D=6 V_0, the beam diameter was focused to smaller than 0.5 mm. In the practical experiment, we chose the spot size of between 1 and 2 mm.

A electron gun designed by Stoffel and Johnson [53] can also be used. This electron gun comprised of a dynode for electron extraction and a retarding three-element-lens. The latter electrostatic lens possesses the focusing property. However, we found that this electron gun generates slightly higher background photons in the visible and near-ultraviolet range than the Erdman-Zipf type gun. The stray photons are probably generated at the anode electrode hit by stray electrons; the anode potential is higher in the Stoffel-Johnson electron gun ($6\,V_0$) than in the Erdman-Zipf electron gun (0.6-0.8 V_0).

The energy spread of electrons was measured as the first derivative of the sample current with respect to the electron kinetic energy as shown in Figure 3 (panels c and d). The width in a full width at a half maximum, FWHM, was 0.23 eV which is in a good agreement with the value predicted from the cathode temperature.

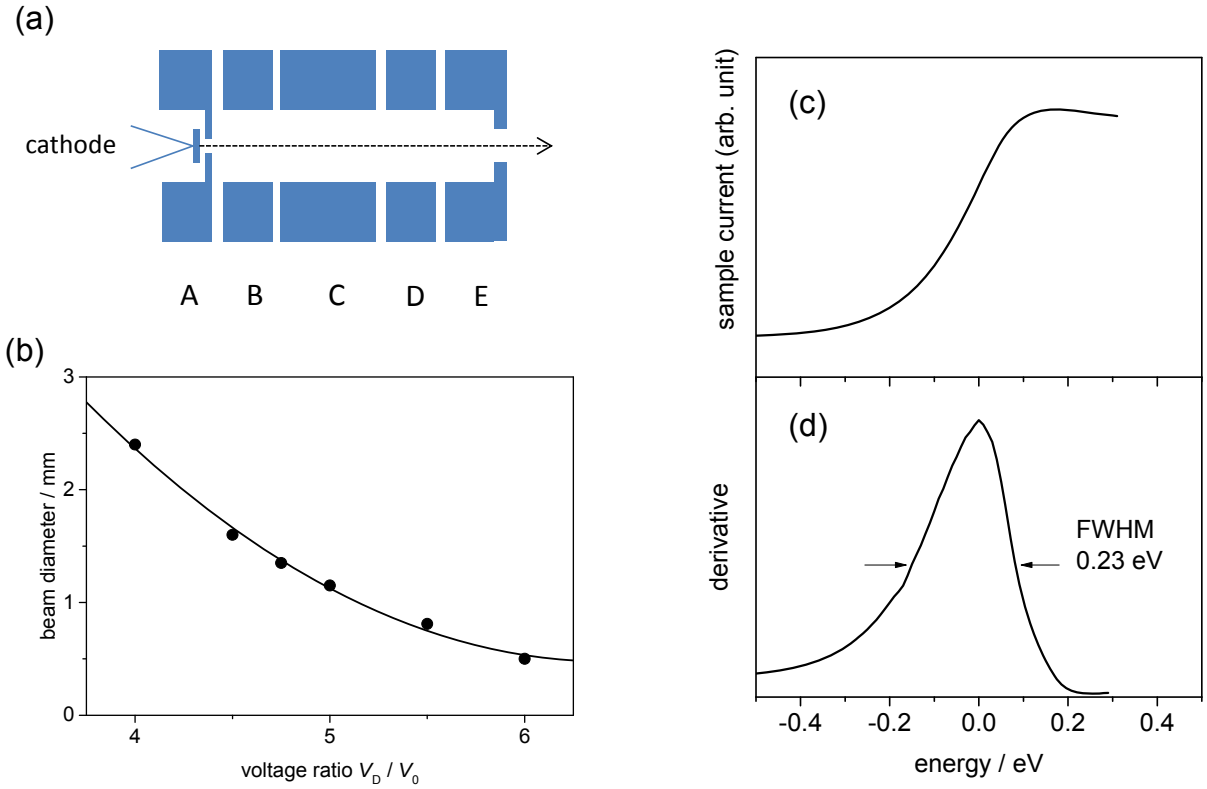

Fig. 3: a) Schematic diagram of Erdman-Zipf electron gun. b) The beam diameter at 20 mm downstream from the exit aperture E as a function of ratio between the potential V_D of electrode D and the beam energy V_0. The solid line is a guide to the eyes. Note that $V_D=4\,V_0$ is recommended in the original literature. (c) The sample current on the polycrystalline Ag thin film as a function of electron kinetic energy. (d) The first derivative of the sample current showing the energy spread of the electron beam.

3.2 Photon detector

In contrast to the VUV photons, various optics are available for the NUV photons such as lenses and windows of quartz, aluminum-coated mirrors and gratings, photomultipliers. Further, the NUV light is not absorbed by oxygen and can be handled in air. These facilitate design and construction of the photon detectors.

For the selection of the NUV photons, an interference bandpass filter which consists of multilayers of dielectric materials having different refractive indices. Thus the bandpass property can be tuned with higher freedom than the VUV bandpass detector used for VUV-IPES. The FWHM of passband is as narrow as 0.05 eV, and the center energy can be varied from NUV (typically 250 nm) to near infrared range. The transmittance in the passband is more than 65% in the NUV range and 80% in the

visible range. Combining the bandpass filter with a photomultiplier having a low dark current, photons can be detected with high resolution and sensitivity for LEIPS.

An apparatus based on the bandpass filter is shown in Figure 4a [54]. Using this setup, the LEIPS spectrum of a CuPc film was measured as shown in Figure 5a. The spectral line shape does not vary depending on the photon energy [25]. This observation confirms that the spectrum is not affected by the initial state and reflects the density of unoccupied states of the CuPc film.

There are many commercially available spectrometers in the visible and NUV range. We demonstrate that these instruments can be used for the analysis of photons in LEIPS measurement [55]. In Figure 4b, the LEIPS setup using a Czerny-Turner spectrometer is compared with the VUV-IPES apparatus using the spectrometer (Figure 4c). In the VUV range, the concave or toroidal grating is used in order to avoid low-reflectivity mirrors. The photon detection should be made in the vacuum. Thus the instrument is specially designed and built in the vacuum. In contrast, the LEIPS apparatus shown in Figure 4b consists of a commercial spectrometer and optics, and the photon detection system is built in air. The tuning and maintenance is much easier.

Figure 5b shows the spectrum of CuPc taken at a fixed photon energy of 4.13 eV (300 nm) in the isochromat mode. The spectrum is similar to that measured using the bandpass filter. Since the collection efficiency of the photon and the transmittance of the monochrometer (40%) were low, however, the measurement for the entire spectral range took 11 hours. This can be compensated by detecting the energy-dispersed photons simultaneously by a CCD detector. Such a spectrum taken with the photon energy ranging between 250 and 370 nm at the fixed electron energy of 0.97 eV in the TPE mode is shown in Figure 5c. The duration required for the sufficient signal-to-noise ratio was reduced to 2 hours.

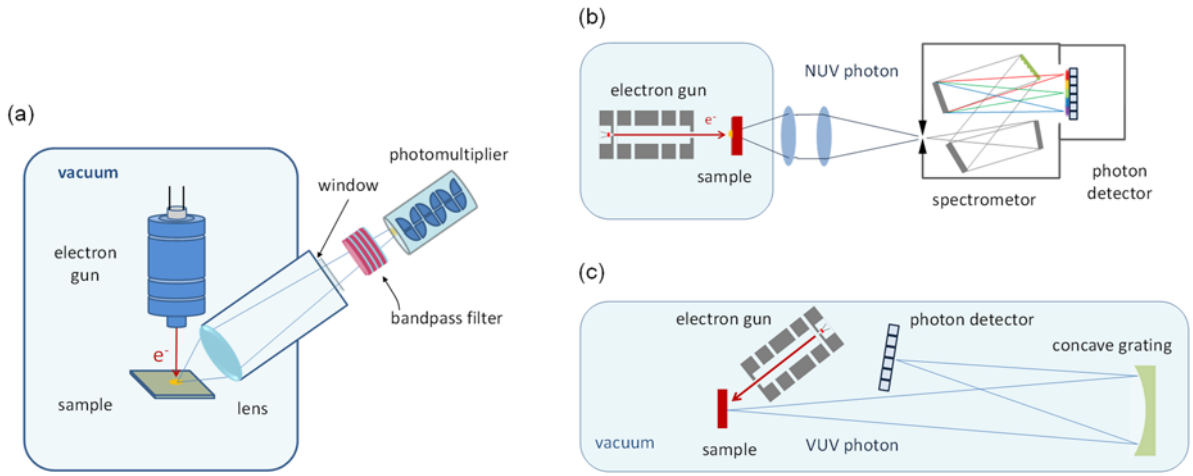

Fig 4: Schematic diagrams of the LEIPS apparatus where photons are analyzed using a) a bandpass filter [54] and b) a spectrometer with the Czerny-Turner configuration [55]. c) The earlier IPES apparatus using the spectrometer shown for comparison.

3.3 Performance of LEIPS

In order to assess the sample damage by the electron bombardment, we measured the CuPc film repeatedly and examined change of the spectra. Figure 6a shows the spectra taken under typical condition of LEIPS, i.e. the electron energy was scanned from 0 to 4 eV. No discernible spectral change was observed even after the 14 hours of continuous spectral scans showing that the CuPc film was not damaged. On the other hand, the spectral line shape apparently changes only after 10 min of the electron bombardment at 10 eV which is similar condition as the VUV-IPES. CuPc is known as among the most durable organic materials [56]. Other organic molecules are expected to be damaged more easily during the measurement of VUV-IPES.

The overall energy resolution is estimated from the width of the image potential state of highly oriented pyrolytic graphite (HOPG) surface. Since the width of the image potential state is smaller than the energy resolution of the LEIPS apparatus, the observed width gives a good estimate of the overall resolution. Figure 7 shows the LEIPS spectra of image potential state measured using bandpass filters with different transmission properties which are shown by the shaded areas. When the bandpass filter having the FWHM of 0.21 eV (panel a) is used, the overall energy resolution is 0.34 eV in FWHM while it is improved to 0.25 eV for the bandpass filter with the FWHM of 0.05 eV (panel b). The overall resolution of IPES is expressed by the convolution of the sensitivity curve of photon detector and the energy distribution of incident electrons. Since the energy spread of incident electron is about 0.23 eV, the overall resolutions are in excellent agreement with the prediction confirming the apparatus works correctly.

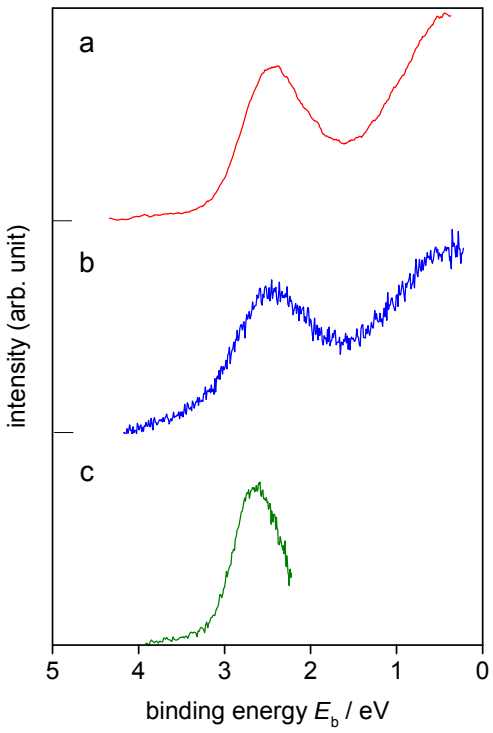

Fig. 5: LEIPS spectra of CuPc measured using a) the bandpass filter (center energy 4.38 eV with the FWHM of 0.21 eV) [25], b) the Czerny-Turner spectrometer at the fixed photon energy of 4.13 eV in the isochromat mode, [55] and c) the Czerny-Turner spectrograph observing the wavelength range between 250 and 370 nm at the fixed electron energy of 0.97 eV in the TPE mode. [55] In the TPE mode, the sensitivity of the photon detector is not calibrated and may depend on the photon energy casing the distortion of the peak shape.

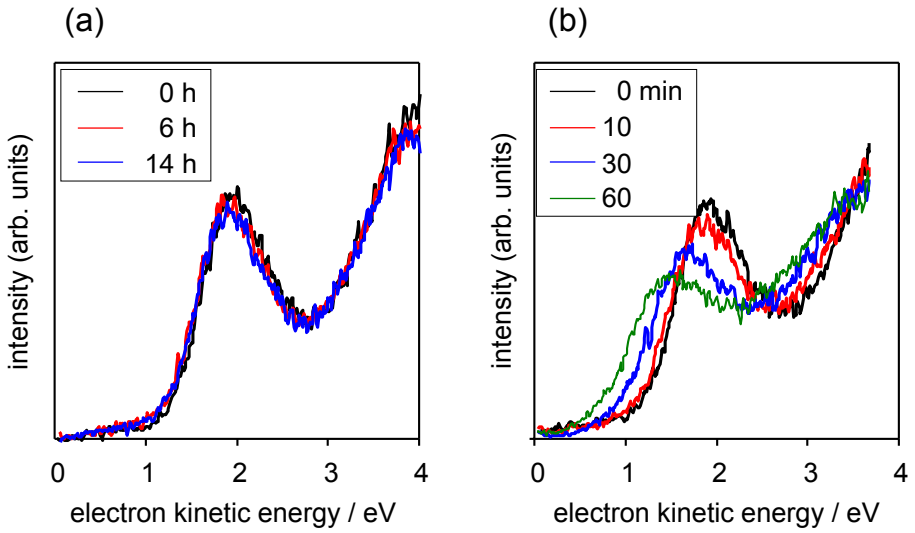

Figure 6: Time dependence of LEIPS spectra showing the radiation damage of a CuPc film [25]. (a) The spectra taken under typical experimental conditions of LEIPS. (b) Spectra taken after electron irradiations of 10 eV in kinetic energy with 1.4 μA in current. This condition represents a usual VUV-IPES measurement.

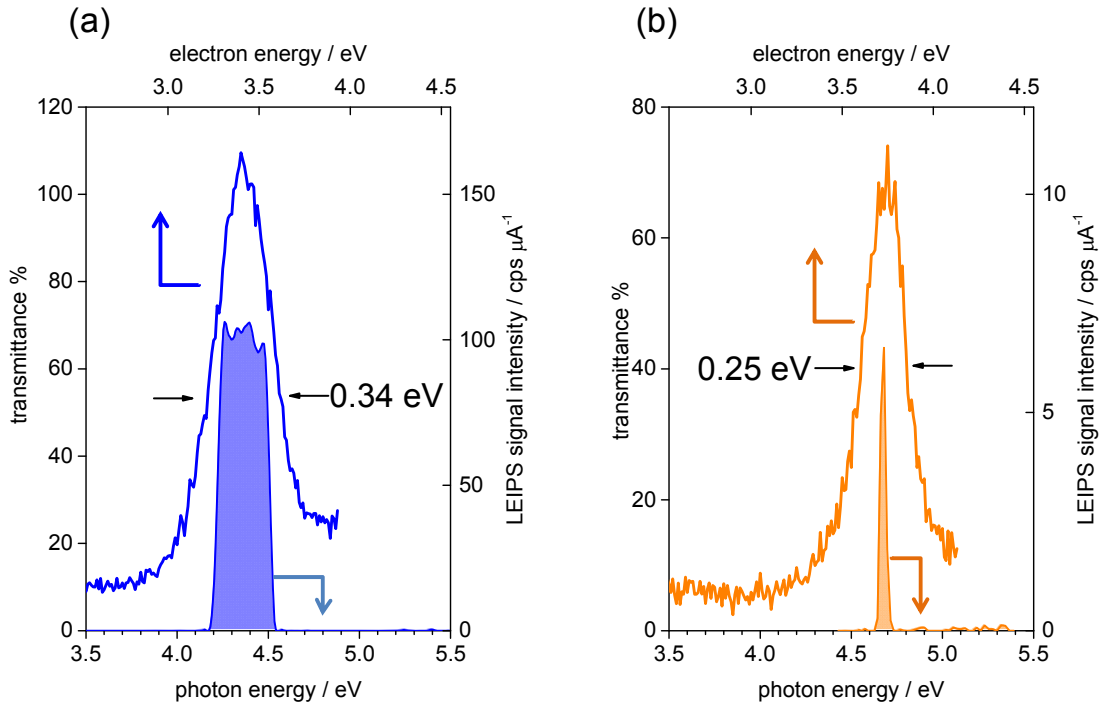

Figure 7: The LEIPS spectra of the image potential state regions of HOPG (solid line) together with the transmittance curve of the bandpass filter used for the measurement (shaded area) [57]. The transmittance of the bandfilters are (a) at the center energy of 4.38 eV with the FWHM of 0.21 eV and (b) the center energy of 4.67 eV with the FWHM 0.05 eV.

4. Examples of LEIPS

4.1 Precise determination of electron affinities

Figure 8a shows LEIPS spectra of a 15 nm-thick perylene-3,4,9,10-tetracarboxylic dianhydride (PTCDA) film at various photon energies $h\nu$. The abscissa is the kinetic energy of electron E_k the origin of which is taken at the maximum of the first derivative of the sample current (see Figure 3d). The onset energy E_k is determined as the crossing point of the two straight lines fitted to onset region of the LUMO-derived peak and the baseline. The electron affinity A is the onset energy with respect to the vacuum level and calculated by $A=h\nu - E_k$.

In order to reduce the systematic error, we use the following procedure [25]: The E_k values are plotted against $h\nu$ as shown in Figure 8b, and the data are fitted to a linear relation with a slope of unity, $E_b=h\nu - E_k$. The electron affinity A is derived by extrapolating E_k to zero (or similarly, $h\nu$ to zero but the sign is opposite). In PTCDA, A is determined to be 4.11 eV.

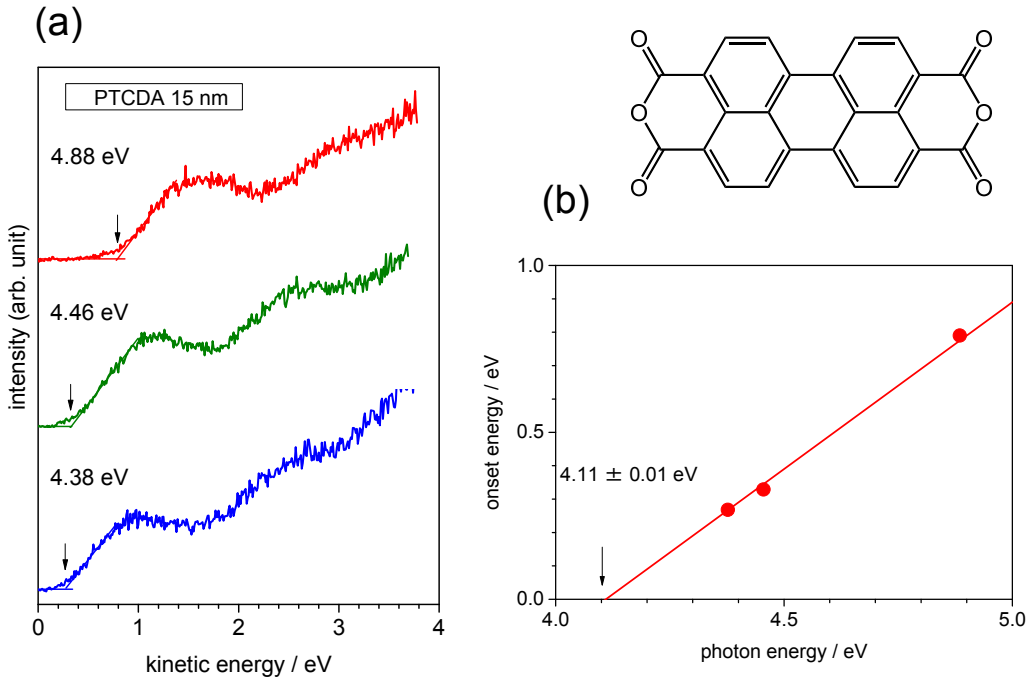

Figure 8: a) LEIPS spectra of a 15 nm-thick PTCDA film at photon energies indicated in the panel. The film was prepared on an ITO glass by vacuum deposition. b) The onset kinetic energy of the LUMO-derived peak is plotted against the photon energy to determine the electron affinity.

Using this procedure, we have determined the electron affinities of typical organic

semiconductors, tris(4-carbazoyl-9-ylphenyl)amine (TCTA), 4,4'-bis(carbazol-9-yl)biphenyl (CBP), 8-hydroxyquinolinolato-lithium (Liq), tris(2-phenylpyridinato)iridium(III) ($Ir(ppy)_3$), (2,9-dimethyl-4,7-diphenyl-1,10-phenanthroline) (BCP), tris(8-hydroxyquinolinato)aluminum (Alq_3), 1,2,3,5-tetrakis(carbazol-9-yl)-4,6-dicyanobenzene (4CzIPN) [58], pentacene [59, 60], CuPc [25], C_{60}, C_{70}, [6,6]-phenyl-C_{61}-butyric acid methyl ester($PC_{61}BM$), [6,6]-phenyl-C_{71}-butyric acid methyl ester($PC_{71}BM$), [6,6]-diphenyl-C_{62}-bis(butyric acid methyl ester)(bis-PCBM), indene-C_{60} bisadduct (ICBA)[61, 62], P(NDI2OD-T2), and PDI-CN2[63]. The electron affinities are compiled in Table 1. The data may be compared with those obtained by the conventional IPES. [64] The difference in the onset energies (and electron affinities) between the present and previous IPES is mainly caused by the sample damage rather than the energy resolution. The experimentally obtained spectral line shape is the convolution of the true spectrum with the apparatus function. The effect of the energy resolution on the electron affinity of organic material is limited to less than 0.1 eV when the energy resolution is 0.4-0.5 eV. [6, 16] The sample damage due to the electron bombardment varies one or two orders of magnitude depending on the sample molecules, which is extensively discussed in relation with transmission electron microscopy.[56]

The uncertainties in Table 1 are statistically calculated from the data taken at different photon energies. In addition to statistical error of a particular sample, the electron affinities of organic films as well as the ionization energies generally vary from sample to sample by about ±0.1 eV. This is exemplified by the difference of 3.76 eV [62] and 3.84 eV [61] in the $PC_{61}BM$ data of as-prepared films. The electron affinity depends on the structure of film. For example, the electron affinity of $PC_{61}BM$ film decreases by 0.1-0.2 eV when the crystallinity of the film increases.[62] Further, the energy levels of the crystalline organic films depend on the molecular orientation.[4] This is clearly demonstrated by the difference in electron affinities of pentacene, 2.35 eV for the standing orientation, 2.70 eV for the disordered film and 3.14 eV for the lying orientation. The orientation dependent electron affinities of perfluoropentacene, picene, α-sexithiophene (6T) will be reported elsewhere [60, 65].

TCTA, CBP, $Ir(ppy)_3$, BCP, and Alq_3 are standard materials for organic light-emitting diodes (OLEDs) whose electron affinities were observed in the range between 1.6 and 2.1 eV. The frequently referred values for the electron affinities were determined from the optical gaps and the ionization energies to be 2.4 eV[66] (TCTA), 3.0 eV[67] (CBP), 3.0 eV[67] ($Ir(ppy)_3$), 3.2 eV[67] (BCP) and 3.3 eV[67] (Alq_3). These values are by about

1 eV larger than that determined by LEIPS. A modern OLED consists of multilayers and the energy level alignment between the layers are crucial to increase the efficiency and decrease the operation voltage. Such large discrepancies in the electron affinities urge reconsideration of the energy level alignment of unoccupied states and electron injection barriers in OLED.

Organic photovoltaic cells (OPVs) consist of the electron donor and acceptor, and the charge generation takes place at the interface of the two layers. Fullerene and its derivatives, C_{60}, C_{70}, $PC_{61}BM$, bis-PCBM, and ICBA are frequently used for the electron accepting layer. The precise value of electron affinity for the acceptor material is important to the operation of OPV. For example, the open circuit voltage V_{oc} of OPV is connected with the difference between the ionization energy of donor I_d and the electron affinity of acceptor A_a. In OPV studies, the I_d and A_a values are often derived from the oxidation and reduction potentials measured in solution using cyclic voltammetry (CV), respectively. Based on the CV data, the following relation is proposed and widely accepted,

$$V_{oc} = I_d - A_a - \Delta,$$

where Δ is constant ranging between 0.3 and 0.5 eV [68]. However, we found that Δ depends linearly on the difference $(I_d - A_a)$ when the I_d and A_a values are determined for the solid samples (films) using UPS and LEIPS, respectively [61].

We also found that the I_d and A_a values determined by CV sometimes fails to explain the performance of OPV while those by UPS and LEIPS can [69]. These examples clearly demonstrate that the precisely determined electron affinity in the film, representing the electron transport level in the actual device, is necessary for detailed analysis of the device performance.

Table 1: The compiled electron affinities of typical organic semiconductors. The uncertainties are calculated statistically (see text). The thicknesses are given for the vacuum deposited films while the concentrations and solvents are indicated in the parentheses for the spin-coated films. For substrates, ITO has device-grade flatness while ITO/SiO_2 is 10 or 20 nm-thick indium tin-oxide layer formed on a quartz glass plate [25] and may have higher roughness than ITO. SiO_2 is a silicon wafer covered with a native oxide layer while HOPG stands for highly oriented pyrolytic graphite.

material	electron affinity / eV		thickness / nm	substrate	reference	note
TCTA	1.59	± 0.09	5	ITO	[58]	
CBP	1.75	± 0.05	5	ITO	[58]	
Liq	1.85	± 0.06	5	ITO	[58]	
$Ir(ppy)_3$	1.86	± 0.05	5	ITO	[58]	
BCP	1.89	± 0.04	5, 25	ITO	[58]	
Alq_3	2.06	± 0.03	5	ITO	[58]	
pentacene	2.35	± 0.02	5, 10	SiO_2	[60]	standing orientation
pentacene	2.70	± 0.03	10	ITO/SiO_2	[59]	disordered
4CzIPN	2.81	± 0.05	5	ITO	[58]	
CuPc	3.09	± 0.05	10, 20	ITO/SiO_2	[25]	half of the bandpass width is subtracted in the value in Ref [25].
pentacene	3.14	± 0.02	5, 10	HOPG	[60]	lying orientation
ICBA	3.48	± 0.03	(0.2-0.4% chlorobenzene)	ITO/SiO_2	[61]	
bis-PCBM	3.59	± 0.04	(0.2-0.4% chlorobenzene)	ITO/SiO_2	[61]	
$PC_{61}BM$	3.64	± 0.01	(0.3% chlorobenzene)	ITO	[62]	annealed at 150°C
$PC_{61}BM$	3.76	± 0.02	(0.3% chlorobenzene)	ITO	[62]	as-prepared
$PC_{61}BM$	3.84	± 0.04	(0.4-0.5% chlorobenzene)	ITO/SiO_2	[61]	as-prepared
$PC_{71}BM$	3.81	± 0.06	(0.5% chlorobenzene)	ITO/SiO_2	[61]	
P(NDI2OD-T2)	3.79	± 0.05	5, 20 nm (0.2% chloroform)	ITO	[63]	
C_{60}	3.98	± 0.06	10, 15	ITO/SiO_2	[61]	
C_{70}	4.00	± 0.04	10, 15	ITO/SiO_2	[61]	
PDI-CN2	4.09	± 0.04	5, 20 nm (0.2% chloroform)	ITO	[63]	
PTCDA	4.11	± 0.01	15	ITO/SiO_2	this paper	lying orientation

4.2 Determining the contribution of electronic polarization energy

The electronic states of organic semiconductors are affected by many factors such as electronic polarization energy [70], surface dipole[71, 72], molecular orientation[4], doping level [73], and bandwidth (intermolecular interaction)[3]. It was normally difficult to distinguish contributions of these effects. We have demonstrated that precise values of both ionization energy and electron affinity allow us to identify the origin of energy level changes associated with the crystallization of PCBM film [74].

PCBM films are usually prepared by spin coating. The as-prepared film is amorphous and crystallized when the film is annealed at 150°C for 5 min. We precisely determined the ionization energies, electron affinities, and C1s core levels using ultraviolet photoemission spectroscopy (UPS), LEIPS, and X-ray photoemission spectroscopy (XPS), respectively. The results are schematically shown in Figure 9.

The electronic polarization is energy to stabilize a localized charge carrier by the electronic polarization of surrounding neutral molecules. Thus, roughly speaking, the increase of the polarization energy results in decrease of ionization energy and increase of electron affinity, i.e. narrowing the bandgap. Similarly, the increase of intermolecular interaction narrows the bandgap though it does not affect the core levels. On the other hand, the surface dipole and doping level make rigid shift of occupied and unoccupied states, i.e. increase (or decrease) of both the ionization energy and electron affinity without changing the bandgap. Though the origin of the molecular orientation dependence has not yet been clarified, the orientation dependence also makes the rigid shift. [60, 75]

Based on this idea, the difference of the energy levels between the amorphous and crystalline film of PCBM shown in Figure 9 can be viewed as a superposition of narrowing of band gaps by 0.09 eV and upward rigid shift by 0.17 eV. Since the C1s core level and ionization energy changes in the same magnitude, the change of the intermolecular interaction is small. The origin of the band gap narrowing should be attributed to the increase of the electronic polarization energy upon the crystallization. The rigid shift may originate from the dipole layer due to the reorientation of the PCBM molecule or de-doping of oxygen included during the film preparation.

In order to further confirm the effect of the electronic polarization, we have examined the thickness and density of the sample films using X-ray reflection technique. The X-ray reflection patterns (not shown) show clear oscillation from which we determined

that the thickness decreased by (2.54 ± 0.60)% and the density increased by (2.58 ± 1.5)% upon the crystallization of the PCBM film. The number density of molecule N and electronic polarization energy P are connected by a simple model accounting for the average molecular polarizability α,

$$P = 8.25\, e^2\, \alpha N^{4/3}$$

where e is the charge of electron [70]. Associated with the increase of film density by 2.58%, this equation gives 4% increase in the polarization energy corresponding to the increase of 0.05 eV in each of the ionization energy and electron affinity. The resultant decrease of the bandgap by 0.1 eV is in a good agreement with the above experimental value meaning that the origin of the bandgap narrowing is certainly caused by the increase of electronic polarization energy associated with the densification of the film. Note that origins of such energy level changes are often discussed in terms of an effect somehow arbitrary chosen from polarization energy, intermolecular interaction or doping without sufficient experimental evidence.

Precise value of electron affinity determined by LEIPS gives a clue to identify the origin that contributes to the energy levels of organic semiconductors. This idea is extended to elucidate the origin of the orientation dependence of ionization energy and electron affinity of organic molecular films. [60]

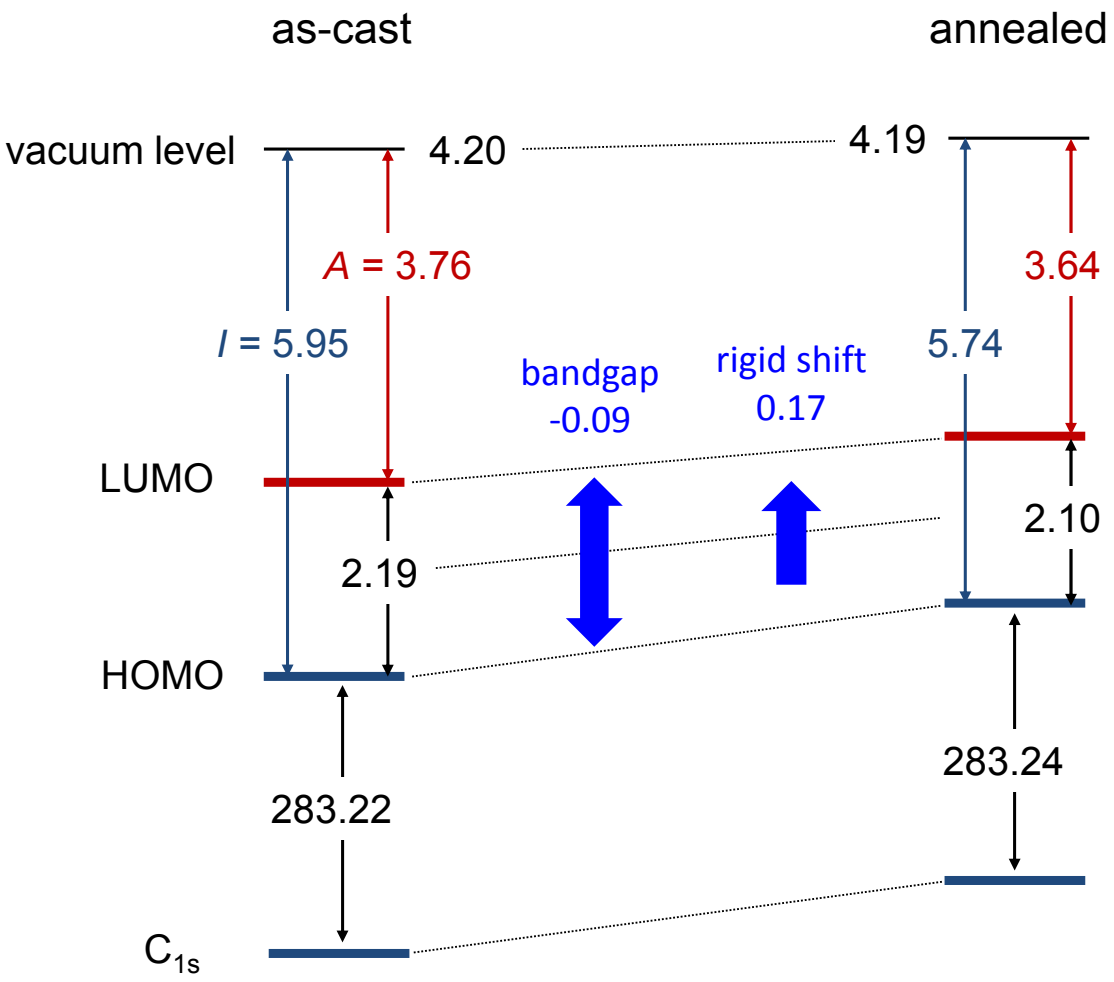

Figure 9: Energy level diagram of PCBM films comparing the as-cast and annealed samples. [62] All energies are in eV. The reference of vacuum level is the Fermi level. The energies of edges of HOMO and LUMO levels with respect to the vacuum level are ionization energy I and electron affinity A, respectively.

5. Summary

We presented low-energy inverse photoemission spectroscopy (LEIPS), a new experimental method to examine the unoccupied state of organic semiconductor. Unlike the VUV-IPES, the damage to organic samples are negligible, and the energy resolution is 0.25 eV, so it becomes possible to examine the unoccupied states of organic materials with the same precision as PES for the ionization energy. Further, building the apparatus is easier than VUV-IPES because the photon analysis can be carried out in air taking advantage of the commercially available devices. The LEIPS will be widely used as a standard analytical method for organic electronics.

Acknowledgements

The author thanks Mr. Yamada, Dr. Richard Murdey, and Professor Naoki Sato of Kyoto University for helpful discussion. This work is supported by JST PRESTO, JST A-STEP, JST ALCA and JSPS KAKENHI (Grant Number 26288007).

References

[1] H. Ishii, K. Sugiyama, E. Ito, K. Seki, Energy level alignment and interfacial electronic structures at organic metal and organic organic interfaces, Adv. Mater., 11 (1999) 605-625.

[2] S. Braun, W.R. Salaneck, M. Fahlman, Energy-level alignment at organic/metal and organic/organic interfaces, Adv. Mater., 21 (2009) 1450-1472.

[3] N. Ueno, S. Kera, Electron spectroscopy of functional organic thin films: Deep insights into valence electronic structure in relation to charge transport property, Prog. Surf. Sci., 83 (2008) 490-557.

[4] S. Duhm, G. Heimel, I. Salzmann, H. Glowatzki, R.L. Johnson, A. Vollmer, J.P. Rabe, N. Koch, Orientation-dependent ionization energies and interface dipoles in ordered molecular assemblies, Nat. Mater., 7 (2008) 326-332.

[5] K. Seki, K. Kanai, Development of experimental methods for determining the electronic structure of organic materials, Mol. Cryst. Liquid Cryst., 455 (2006) 145-181.

[6] H. Yoshida, Measuring the electron affinity of organic solids: an indispensable new tool for organic electronics, Anal. Bioanal. Chem., 406 (2014) 2231-2237.

[7] A. Otto, K.H. Frank, B. Reihl, Inverse photoemission of pyridine on silver(111), Surf. Sci., 163 (1985) 140-152.

[8] K.H. Frank, R. Dudde, E.E. Koch, Electron-affinity levels of benzene and azabenzenes on Cu(111) and Au(110) revealed by inverse photoemission, Chem. Phys. Lett., 132 (1986) 83-87.

[9] K.H. Frank, P. Yannoulis, R. Dudde, E.E. Koch, Unoccupied molecular-orbitals of aromatic-hydrocarbons adsorbed on Ag(111), J. Chem. Phys., 89 (1988) 7569-7576.

[10] P. Yannoulis, K.H. Frank, E.E. Koch, Electronic-structure and orientation of anthracene on Ag(111), Surf. Sci., 241 (1991) 325-334.

[11] R. Dudde, B. Reihl, Complete electronic-structure of oriented films of hexatriacontane, Chem. Phys. Lett., 196 (1992) 91-96.

[12] Y. Hirose, C.I. Wu, V. Aristov, P. Soukiassian, A. Kahn, Chemistry and electronic properties of metal contacts on an organic molecular semiconductor, Appl. Surf. Sci., 113 (1997) 291-298.

[13] C.I. Wu, Y. Hirose, H. Sirringhaus, A. Kahn, Electron-hole interaction energy in the organic molecular semiconductor PTCDA, Chem. Phys. Lett., 272 (1997) 43-47.

[14] N. Sato, H. Yoshida, K. Tsutsumi, Photoemission and inverse photoemission studies

on a thin film of N,N '-dimethylperylene-3,4,9,10-bis(dicarboximide), J. Electron Spectrosc. Relat. Phenom., 88 (1998) 861-865.
[15] M. Gorgoi, W. Michaelis, T.U. Kampen, D. Schlettwein, D.R.T. Zahn, Thickness dependence of the LUMO position for phthalocyanines on hydrogen passivated silicon (111), Appl. Surf. Sci., 234 (2004) 138-143.
[16] S. Krause, M.B. Casu, A. Scholl, E. Umbach, Determination of transport levels of organic semiconductors by UPS and IPS, New J. Phys., 10 (2008) 085001.
[17] T. Nishi, T. Iwahashi, H. Yamane, Y. Ouchi, K. Kanai, K. Seki, Electronic structures of ionic liquids $[C_nmim]^+$ BF_4^- and $[C_nmim]^+$ PF_6^- studied by ultraviolet photoemission, inverse photoemission, and near-edge X-ray absorption fine structure spectroscopies, Chem. Phys. Lett., 455 (2008) 213-217.
[18] K. Tsutsumi, H. Yoshida, N. Sato, Unoccupied electronic states in a hexatriacontane thin film studied by inverse photoemission spectroscopy, Chem. Phys. Lett., 361 (2002) 367-373.
[19] Z. Li, S.Q. Sun, X. Li, R. Schlaf, The impact of inverse photoemission spectroscopy measurements on regioregular poly(3-hexylthiophene) films, Appl. Phys. Lett., 104 (2014) 021606.
[20] D.R.T. Zahn, G.N. Gavrila, M. Gorgoi, The transport gap of organic semiconductors studied using the combination of direct and inverse photoemission, Chem. Phys., 325 (2006) 99-112.
[21] R. Murdey, N. Sato, M. Bouvet, Frontier electronic structures in fluorinated copper phthalocyanine thin films studied using ultraviolet and inverse photoemission spectroscopies, Mol. Cryst. Liquid Cryst., 455 (2006) 211-218.
[22] H. Yoshida, K. Tsutsumi, N. Sato, Unoccupied electronic states of 3d-transition metal phthalocyanines (MPc: M=Mn, Fe, Co, Ni, Cu and Zn) studied by inverse photoemission spectroscopy, J. Electron Spectrosc. Relat. Phenom., 121 (2001) 83-91.
[23] J.B. Pendry, New probe for unoccupied bands at surfaces, Phys. Rev. Lett., 45 (1980) 1356-1358.
[24] V. Dose, VUV isochromat spectroscopy, Applied Physics, 14 (1977) 117-118.
[25] H. Yoshida, Near-ultraviolet inverse photoemission spectroscopy using ultra-low energy electrons, Chem. Phys. Lett., 539-540 (2012) 180-185.
[26] J.K. Lang, Y. Baer, Bremsstrahlung isochromat spectroscopy using a modified XPS apparatus, Rev. Sci. Instrum., 50 (1979) 221-226.
[27] G. Denninger, V. Dose, H. Scheidt, VUV isochromat spectrometer for surface-analysis, Applied Physics, 18 (1979) 375-380.
[28] V. Dose, T. Fauster, R. Schneider, Improved resolution in VUV isochromat spectroscopy, Appl. Phys. A-Mater. Sci. Process., 40 (1986) 203-207.
[29] D. Funnemann, H. Merz, 10 eV photon detector for inverse photoemission, Journal

of Physics E-Scientific Instruments, 19 (1986) 554-557.
[30] J.A. Lipton-Duffin, A.G. Mark, A.B. McLean, Photon detection with n-propanol and C2H6O isomers, Rev. Sci. Instrum., 73 (2002) 3149-3153.
[31] J.A. Lipton-Duffin, A.G. Mark, G.K. Mullins, G.E. Contant, A.B. McLean, An inverse photoemission system with large solid angle of detection and adjustable optical bandpass, Rev. Sci. Instrum., 75 (2004) 445-454.
[32] R. Stiepel, R. Ostendorf, C. Benesch, H. Zacharias, Vacuum ultraviolet photon detector with improved resolution for inverse photoemission spectroscopy, Rev. Sci. Instrum., 76 (2005) 063109.
[33] M. Budke, V. Renken, H. Liebl, G. Rangelov, M. Donath, Inverse photoemission with energy resolution better than 200 meV, Rev. Sci. Instrum., 78 (2007) 083903.
[34] M. Maniraj, S.W. D'Souza, J. Nayak, A. Rai, S. Singh, B.N.R. Sekhar, S.R. Barman, High energy resolution bandpass photon detector for inverse photoemission spectroscopy, Rev. Sci. Instrum., 82 (2011) 093901.
[35] N. Babbe, W. Drube, I. Schafer, M. Skibowski, A simple and compact system for combined angular resolved inverse photoemission and photoemission in the vacuum ultraviolet, Journal of Physics E-Scientific Instruments, 18 (1985) 158-160.
[36] H. Namatame, M. Tamura, M. Nakatake, H. Sato, Y. Ueda, M. Taniguchi, M. Fujisawa, High-resolution band-pass photon detector for inverse-photoemission spectroscopy, J. Electron Spectrosc. Relat. Phenom., 80 (1996) 393-396.
[37] F. Schedin, G. Thornton, R.I.G. Uhrberg, Windows and photocathodes for a high resolution solid state bandpass ultraviolet photon detector for inverse photoemission, Rev. Sci. Instrum., 68 (1997) 41-46.
[38] G. Chauvet, R. Baptist, Inverse photoemission spectrometer in the range 20-100 eV, J. Electron Spectrosc. Relat. Phenom., 24 (1981) 255-265.
[39] T. Fauster, F.J. Himpsel, J.J. Donelon, A. Marx, Spectrometer for momentum-resolved Bremsstrahlung spectroscopy, Rev. Sci. Instrum., 54 (1983) 68-75.
[40] T. Fauster, D. Straub, J.J. Donelon, D. Grimm, A. Marx, F.J. Himpsel, Normal-incidence grating spectrograph with large acceptance for inverse photoemission, Rev. Sci. Instrum., 56 (1985) 1212-1214.
[41] P.D. Johnson, S.L. Hulbert, R.F. Garrett, M.R. Howells, Normal incidence grating spectrometer designed for inverse photoemission-studies in the range 10-30 eV, Rev. Sci. Instrum., 57 (1986) 1324-1328.
[42] P.T. Andrews, Inverse photoemission, Vacuum, 38 (1988) 257-260.
[43] Y. Gao, M. Grioni, B. Smandek, J.H. Weaver, T. Tyrie, Inverse photoemission spectrometer for interface studies, Journal of Physics E-Scientific Instruments, 21 (1988) 489-494.
[44] M. Sancrotti, L. Braicovich, C. Chemelli, F. Ciccacci, E. Puppin, G. Trezzi, E.

Vescovo, Ultraviolet inverse photoemission spectrograph with parallel multichannel isochromat acquisition, Rev. Sci. Instrum., 62 (1991) 639-642.
[45] T.E. Ollonqvist, I.J. Vayrynen, Normal incidence grating spectrometer for inverse-photoemission, Vacuum, 46 (1995) 1177-1180.
[46] L. Kipp, M. Boehme, H. Carstensen, R. Claessen, M. Skibowski, Compact grating spectrometer for inverse photoemission spectroscopy, Rev. Sci. Instrum., 68 (1997) 2144-2148.
[47] M.B. Jost, N. Troullier, D.M. Poirier, J.L. Martins, J.H. Weaver, L.P.F. Chibante, R.E. Smalley, Band dispersion and empty electronic states in solid C_{60} - inverse photoemission and theory, Phys. Rev. B, 44 (1991) 1966-1969.
[48] M.B. Jost, P.J. Benning, D.M. Poirier, J.H. Weaver, L.P.F. Chibante, R.E. Smalley, Occupied and unoccupied electronic states of solid C_{70} with comparison to C_{60}, Chem. Phys. Lett., 184 (1991) 423-427.
[49] A. Kahn, N. Koch, W.Y. Gao, Electronic structure and electrical properties of interfaces between metals and pi-conjugated molecular films, Journal of Polymer Science Part B-Polymer Physics, 41 (2003) 2529-2548.
[50] P.I. Djurovich, E.I. Mayo, S.R. Forrest, M.E. Thompson, Measurement of the lowest unoccupied molecular orbital energies of molecular organic semiconductors, Org. Electron., 10 (2009) 515-520.
[51] B. Boudaiffa, P. Cloutier, D. Hunting, M.A. Huels, L. Sanche, Resonant formation of DNA strand breaks by low-energy (3 to 20 eV) electrons, Science, 287 (2000) 1658-1660.
[52] P.W. Erdman, E.C. Zipf, Low-voltage, high-current electron-gun, Rev. Sci. Instrum., 53 (1982) 225-227.
[53] N.G. Stoffel, P.D. Johnson, A low-energy high-brightness electron-gun for inverse photoemission, Nucl. Instrum. Methods Phys. Res. Sect. A-Accel. Spectrom. Dect. Assoc. Equip., 234 (1985) 230-234.
[54] H. Yoshida, Note: Low energy inverse photoemission spectroscopy apparatus Rev. Sci. Instrum., 85 (2014) 016101.
[55] H. Yoshida, Low-energy inverse photoemission spectroscopy using a high-resolution grating spectrometer in the near ultraviolet range, Rev. Sci. Instrum., 84 (2013) 103901.
[56] L. Reimer, in: P.W. Hawkes (Ed.) Transmission Electron Microscopy: Physics of Image Formation and Microanalysis, Springer Series in Optical Sciences, Springer, Berlin, 1997.
[57] K. Yamada, Study on orientation dependence of electronic states investigated as a solid effect on electronic structure of organic semiconductor films: controlling the molecular orientation and precise determination of the electron affinities using low-energy inverse photoemission spectroscopy (in Japanese), Master Thesis, Graduate School of Science, Kyoto University, Kyoto, 2015.

[58] H. Yoshida, K. Yoshizaki, Electron affinities of organic materials used for organic light-emitting diodes: A low-energy inverse photoemission study, Org. Electron., 20 (2015) 24-30.
[59] W. Han, H. Yoshida, N. Ueno, S. Kera, Electron affinity of pentacene thin film studied by radiation-damage free inverse photoemission spectroscopy, Appl. Phys. Lett., 103 (2013) 123303.
[60] H. Yoshida, K. Yamada, J. Tsutsumi, N. Sato, A complete description of ionization energy and electron affinity in organic solids: Determining contributions from electronic polarization, energy band dispersion and molecular orientation, (submitted).
[61] H. Yoshida, Low-energy Inverse Photoemission Study on the Electron Affinities of Fullerene Derivatives for Organic Photovoltaic Cells, J. Phys. Chem. C, 118 (2014) 24377-24382.
[62] Y.F. Zhong, S. Izawa, K. Hashimoto, K. Tajima, T. Koganezawa, H. Yoshida, Crystallization-Induced Energy Level Change of 6,6 -Phenyl C-61-Butyric Acid Methyl Ester (PCBM) Film: Impact of Electronic Polarization Energy, J. Phys. Chem. C, 119 (2015) 23-28.
[63] N. Zhou, M.-G. Kim, S. Loser, J. Smith, H. Yoshida, X. Guo, C. Song, H. Jine, Z. Chen, S.M. Yoon, A.J. Freeman, R.P.H. Chang, A. Facchetti, T.J. Marks, Amorphous oxide alloys as interfacial layers with broadly tunable electronic structures for organic photovoltaic cells, Proceedings of the National Academy of Sciences of the United States of America, (2015).
[64] J. Hwang, A. Wan, A. Kahn, Energetics of metal-organic interfaces: New experiments and assessment of the field, Materials Science & Engineering R-Reports, 64 (2009) 1-31.
[65] K. Yamada, R. Shiraishi, K. Nakao, R. Murdey, N. Sato, R. Makino, Y. Suda, K. Yonezawa, T. Yamaguchi, S. Kera, H. Yoshida, A method to evaluate accurate values of the ionization energy and electron affinity of an organic semiconductor from the electrochemical oxidation and reduction potentials of its component molecule: correction for the electrostatic energy, (submitted).
[66] S.H. Kim, J. Jang, J.Y. Lee, Relationship between host energy levels and device performances of phosphorescent organic light-emitting diodes with triplet mixed host emitting structure, Appl. Phys. Lett., 91 (2007) 083511.
[67] C. Adachi, R. Kwong, S.R. Forrest, Efficient electrophosphorescence using a doped ambipolar conductive molecular organic thin film, Org. Electron., 2 (2001) 37-43.
[68] C.J. Brabec, A. Cravino, D. Meissner, N.S. Sariciftci, T. Fromherz, M.T. Rispens, L. Sanchez, J.C. Hummelen, Origin of the open circuit voltage of plastic solar cells, Adv. Funct. Mater., 11 (2001) 374-380.
[69] Y. Ie, M. Karakawa, S. Jinnai, H. Yoshida, A. Saeki, S. Seki, S. Yamamoto, H.

Ohkita, Y. Aso, Electron-donor function of methanofullerenes in donor-acceptor bulk heterojunction systems, Chem. Comm., 50 (2014) 4123-4125.
[70] N. Sato, K. Seki, H. Inokuchi, Polarization energies of organic-solids determined by ultraviolet photoelectron-spectroscopy, J. Chem. Soc. -Faraday Trans. 2, 77 (1981) 1621-1633.
[71] Q. Wei, K. Tajima, Y. Tong, S. Ye, K. Hashimoto, Surface-Segregated Monolayers: A New Type of Ordered Monolayer for Surface Modification of Organic Semiconductors, J. Am. Chem. Soc., 131 (2009) 17597-17604.
[72] Y. Geng, Q. Wei, K. Hashimoto, K. Tajima, Dipole Layer Formation by Surface Segregation of Regioregular Poly(3-alkylthiophene) with Alternating Alkyl/Semifluoroalkyl Side Chains, Chem. Mater., 23 (2011) 4257-4263.
[73] W. Gao, A. Kahn, Controlled p-doping of zinc phthalocyanine by coevaporation with tetrafluorotetracyanoquinodimethane: A direct and inverse photoemission study, Appl. Phys. Lett., 79 (2001) 4040.
[74] Y. Zhong, S. Izawa, K. Hashimoto, K. Tajima, T. Koganezawa, H. Yoshida, Crystallization-induced energy level change of [6,6]-phenyl-C61-butyric acid methyl ester (PCBM) film: Impact of electronic polarization energy, Journal of Physical Chemistry C, 119 (2015) 23-28.
[75] W.N. Han, K. Yonezawa, R. Makino, K. Kato, A. Hinderhofer, R. Murdey, R. Shiraishi, H. Yoshida, N. Sato, N. Ueno, S. Kera, Quantitatively identical orientation-dependent ionization energy and electron affinity of diindenoperylene, Appl. Phys. Lett., 103 (2013) 253301.

Highlights

- Principle of low energy inverse photoemission spectroscopy is described.
- Instruments including electron sources and photon detectors are shown.
- Recent results about organic devices and fundamental studies are reviewed.
- Electron affinities of typical organic semiconductors are compiled.